

Poleward shift of the major ocean gyres detected in a warming climate

Hu Yang¹, Gerrit Lohmann¹, Uta Krebs-Kanzow¹, Monica Ionita¹, Xiaoxu Shi¹, Dmitry Sidorenko¹, Xun Gong¹, Xueen Chen², Evan J. Gowan¹

¹Climate Sciences, Alfred Wegener Institute, Helmholtz Centre for Polar and Marine Research, Bremerhaven, Germany

²College of Oceanic and Atmospheric Sciences, Ocean University of China, Qingdao, China

Key Points:

- Satellite observations show a consistent poleward shift of the major ocean gyres during the past four decades.
- Due to strong natural variability, most of the observed ocean gyre shifts are not statistically significant.
- Climate model simulations suggest that the observed shift is most likely to be a response to global warming.

Corresponding author: Hu Yang, Gerrit Lohmann, hyang@awi.de, gerrit.lohmann@awi.de

–1–

This article has been accepted for publication and undergone full peer review but has not been through the copyediting, typesetting, pagination and proofreading process, which may lead to differences between this version and the Version of Record. Please cite this article as doi: 10.1029/2019GL085868

Abstract

Recent evidence shows that wind-driven ocean currents, like the western boundary currents, are strongly affected by global warming. However, due to insufficient observations both on temporal and spatial scales, the impact of climate change on large-scale ocean gyres is still not clear. Here, based on satellite observations of sea surface height and sea surface temperature, we find a consistent poleward shift of the major ocean gyres. Due to strong natural variability, most of the observed ocean gyre shifts are not statistically significant, implying that natural variations may contribute to the observed trends. However, climate model simulations forced with increasing greenhouse gases suggest that the observed shift is most likely to be a response of global warming. The displacement of ocean gyres, which is coupled with the poleward shift of extratropical atmospheric circulation, has broad impacts on ocean heat transport, regional sea level rise and coastal ocean circulation.

Plain Language Summary

Ocean circulation plays a vital role in regulating the weather and climate and supporting marine life. Therefore, it is important to understand whether and how it responds to global warming. However, the available observations are currently sparse and short in duration, making it difficult to track the dynamic changes of large-scale ocean circulation. Here, we show for the first time, independent satellite observational evidence demonstrating that the large-scale ocean gyres are moving poleward during the past four decades. Further analysis based on climate models and various other datasets reveal that the poleward shifting of the ocean gyre circulation is most likely to be a consequence of global warming, which so far has not been well recognized by the public and the scientific community.

1 Introduction

Ocean gyres represent large systems of ocean currents which are driven by the wind (Munk, 1950). At the western edge of subtropical gyres are the western boundary currents, which carry warm water from the tropics poleward, contributing to a warm and wet climate on the adjacent mainland. The eastern margins of the subtropical gyres are manifested by upwelling and cold eastern boundary currents. These provide abundant nutrients for marine ecosystems and contribute to maintaining a relatively cold and dry climate on the nearby continents. Due to strong stratification, oceanic productivity is particularly low over the central parts of the subtropical gyres (commonly called ocean deserts), whereas the subpolar gyres are relatively nutrient-rich, sustaining an abundance of marine life. Given the broad impacts of ocean gyres on the climate and ecosystems, it is crucial to understand how they respond to climate change.

In the past few decades, multiple lines of evidence indicate that the large-scale extratropical atmospheric circulation is shifting towards poles under global warming. This evidence includes poleward shifts of westerly winds (Chen et al., 2008), jet streams (Archer & Caldeira, 2008), storm tracks (Yin, 2005), clouds (Norris et al., 2016) and the pattern of precipitation (Scheff & Frierson, 2012). Comparatively, large-scale ocean circulation changes due to global warming is largely uncertain, mostly due to insufficient ocean observations.

As ocean observations are restricted by short duration and sparse coverage, previous research mainly focused on the variability of ocean circulation from a regional perspective (Roemmich et al., 2007, 2016; Wu et al., 2012; Yang, Lohmann, et al., 2016; Foukal & Lozier, 2017). For example, Frankignoul et al. (2001) showed that the position of the Gulf Stream, derived from satellite altimetry in the 1990s, is 50-100 km north of the position estimated from expendable bathythermographs (XBT) during 1954-1998. A south-

ward advance of the Eastern Australian Current (Ridgway, 2007), the Brazil Current front (Goni et al., 2011) and the Antarctic Circumpolar Current front (Sokolov & Rintoul, 2009) have been observed over the Southern Hemisphere. Roemmich et al. (2007, 2016) reported a strengthening of the South Pacific Subtropical Gyre, while Häkkinen and Rhines (2004) and Foukal and Lozier (2017) observed a weakening of the North Atlantic Subpolar Gyre since 1992.

Considering that direct continuous observations of ocean currents are rare, an indirect approach must be adopted to investigate the dynamic changes of large-scale ocean gyres. Under the constraint of geostrophic balance, the Coriolis force induced by ocean flow is balanced by the pressure gradient caused by the difference in sea surface height (SSH). Thus, the centres of the anticyclonic subtropical gyres are characterized by relatively high regional SSH. The centres of the cyclonic subpolar gyres and the Antarctic Circumpolar Current are distinguished by relatively low regional SSH (Munk, 1950). Therefore, the SSH 'hills' and 'valleys' can be used to locate the position of the ocean gyres (Fig. 1a). Moreover, the subtropical gyres represent a circulation of warm water, while the subpolar water is relatively cold. The confluence of the warm subtropical gyres and the cold subpolar gyres generates sharp Sea Surface Temperature (SST) fronts at the mid-latitudes, namely the subtropical fronts. These fronts mark the boundary between the subtropical and subpolar gyres (Fig. 1b).

Satellite altimetry has continuously monitored SSH since late 1992. Satellite based SST records have been collected for almost four decades, starting from the early 1980s. These data are independently observed and provide an unprecedented opportunity to explore the dynamic changes of the large-scale ocean gyres. In the present study, we evaluate the results from both satellite observations and climate simulations and find a consistent poleward shift of the major ocean gyres in a warming climate.

2 Data and Methods

2.1 Data and Simulations

Satellite-based SSH (data from 1992-2018 AVISO) and SST (data from 1982-2018 NOAA OISST) are used to investigate the dynamic changes of ocean gyres. Near surface wind and Sea Level Pressure (SLP) data from the NCEP/NCAR (Kalnay et al., 1996), NCEP-DOE (Kanamitsu et al., 2002) and ERA-Interim reanalysis datasets are included to explore the dynamic mechanism responsible for the ocean circulation changes.

To validate the observational trend, two series of simulations, namely, a pre-industrial control run and a set of doubled CO₂ runs, are conducted by the Alfred Wegener Institute Climate Model (AWI-CM) using the same configuration as in Sidorenko et al. (2015). The pre-industrial control run is integrated for 800 years, forced by greenhouse gas concentrations fixed at the 1850 levels. The doubled CO₂ runs are integrated for 150 years by linearly increasing the concentration of greenhouse gases to a doubled level. The doubled CO₂ runs are performed five times starting from different initial conditions obtained from the pre-industrial control run. To reduce the amplitude of natural climate variability, the ensemble mean of the last 10 years of the doubled CO₂ simulations are then used to compare with the last 100 years of the pre-industrial control run.

Furthermore, to demonstrate that the results are not model dependent, the *piControl* and *1pctCO2* simulations from the fifth phase of the Coupled Model Intercomparison Project (CMIP5) (Taylor et al., 2012) are presented as well in the Supporting Information. Twenty-two climate models are included to obtain an ensemble trend. Detailed information on the models used in this study is summarized in Table S1.

2.2 Methods

As mentioned in the introduction, the gyre centre and gyre boundary are physically associated with the patterns of SSH and SST gradient (Fig. 1). To examine the meridional variations of ocean gyres, we introduce two indices based on these two parameters. Imagine that gyre related SSH patterns resemble shape of 'hills' (the subpolar SSH 'valleys' can be mirrored into 'hills' by subtracting the regional maximum SSH), we use the centre of mass of these 'hills' to identify their position. The detailed computation follows the equation below:

$$P = \frac{\int \Delta var \cdot lat}{\int \Delta var} \quad (1)$$

where P is the meridional location of ocean gyres, lat is the latitudinal coordinate of SSH. Δvar represents $SSH - SSH_{min}$ for calculating the position of subtropical gyres, and $SSH - SSH_{max}$ for calculating the position of subpolar gyres. The SSH_{min} and SSH_{max} denote the regional minimum and maximum SSH within the integrated regions (as shown by grey rectangles in Fig. 3A). These regions are defined primarily based on the climatology position of the gyre centre. They do not vary over time.

In a similar way, the meridional variations of gyre boundaries are also estimated based on the SST gradients. Following Equation 1, here, Δvar denotes the horizontal SST gradient (includes both zonal and meridional components). The integrated regions are given by the grey rectangles in Fig. 4A, following the climatology positions of the subtropical fronts.

To check whether our indices derived from SSH and SST gradients are suitable to locate the ocean gyres, we verified them in our climate model. The results suggest that they are excellent proxies to reconstruct the position of ocean gyres (see section: 'Validation of metrics of ocean gyres position' in Supporting Information).

In the climate model, the meridional positions of the ocean gyres are also estimated following Equation 1, where Δvar denotes the barotropic streamfunction. Here, the integration is performed within the boundary (zero-crossing of barotropic streamfunction) of ocean gyres at each ocean basin. This is different from the approach applied in the observations, in which the integration is performed within the pre-defined regions, because it is hard to find a common threshold to identify the boundary of the ocean gyres in the observations.

3 Poleward shift of the major ocean gyres

3.1 Observational Results

Figs. 3A and 4A present the linear trends (shading) of SSH and SST gradients during the satellite era. Enhanced regional sea level rise is found over the mid-latitude bands in both hemispheres, while the sea level rise over the high latitudes is below the globally averaged trend. Comparing the trend of SSH with its climatology pattern (contours), the enhanced sea level rise over the mid-latitudes illustrates that the subtropical SSH 'hills' and subpolar SSH 'valleys' have shifted towards the poles. Associated with the SSH trend, increasing/decreasing trends of SST gradients are found over polar/equator flanks of the subtropical fronts respectively, implying that the subtropical fronts have a similar signal of poleward displacement.

Fig. 5A shows the interannual variations of the location of the major ocean gyres based on SSH and SST gradients. The time series of both metrics show similar temporal variations in the overlapping period (1993-2018). Moreover, positive trends are found for all the major ocean gyres, illustrating that they are consistently migrating towards

the poles during the past four decades. The average magnitude of the shift is on the order of 0.07° per decade. Most of the Southern Hemisphere ocean gyres (except the Indian Ocean Subtropical Gyre) have experienced a statistically significant poleward shift, while the ocean gyre displacements over the Northern Hemisphere are not statistically significant. These trends are superimposed by strong natural variations. It remains unclear whether the poleward movements are due to natural climate variability or long-term anthropogenic climate change.

3.2 Climate Model results

To address this issue, we compared the observational results with the results from the climate model (AWI-CM). As presented in Figs. 3B and 4B, the ensemble simulations are consistent with the observations showing an enhanced SSH increase over the mid-latitudes. Similarly, there are positive/negative trends of the SST gradients over the polar/equator flanks of the subtropical fronts, respectively. Tracking the meridional position of ocean gyres in the doubled CO_2 simulations (Fig. 5B) illustrates that all the major ocean gyres shift towards the poles. We notice that the North Pacific Subtropical Gyre and the North Pacific Subpolar Gyre have minor poleward shifts in comparison with their strong internal variability.

In addition to our results from AWI-CM, we also carry out a comprehensive analysis on model data from CMIP5 (Taylor et al., 2012). The ensemble results from the *1pctCO2* experiment also show poleward displacement of the ocean gyres (Figs. S1 and S2). The agreement among these broad ranges of observations and climate simulations suggests that poleward migration of the major ocean gyres is most likely to be a response to global warming.

4 Mechanism

According to the theory of ocean circulation, the ocean gyres are driven by near-surface ocean wind, more specifically the wind stress curl (Munk, 1950). To explore the mechanism driving the shift of ocean gyres, we examine the trends of near surface wind and associated SLP. As shown in Fig. 6A, a large portion of subtropical oceans (approximately between 20° - 40° latitude bands) show a change of velocity of the easterly winds, while, there is a change of velocity of the westerly winds over the 40° - 60° latitude bands. Compared with the climatological (contours) pattern of zonal wind, the observational wind pattern change implies that the extratropical atmospheric surface winds have shifted towards higher latitudes during the past four decades. Consequently, the wind stress curl has shifted as well (not shown). In agreement with observations, the ensemble climate model result (Fig. 6B) displays a similar pattern of shifting wind under forcing of increasing CO_2 . We propose that the movement of the near surface wind drives the displacement of the ocean gyres.

A large number of climate simulations have demonstrated that the extratropical atmospheric circulation undergoes a systematic poleward shift under GHG forcing (J. Fyfe et al., 1999; Kushner et al., 2001; Cai et al., 2003; Saenko et al., 2005; J. C. Fyfe & Saenko, 2006; Cai, 2006; Sen Gupta et al., 2009). On one hand, the displacement of the atmospheric circulation can drive the shift in ocean gyres. On the other hand, shifting ocean gyres contribute to moving the subtropical front, which may also alter the atmospheric circulation (Nakamura et al., 2004; Hudson, 2012). Thus, these dynamics are strongly coupled. We believe that the identified shift in ocean gyres is another manifestation of a systematic movement of the entire extratropical climate zone.

5 Discussion and Conclusions

Based on results from satellite observations and climate simulations, we identify a consistent poleward shift of the major ocean gyres in a warming climate. Due to short temporal coverage and strong natural climate variability, most of the observed shifts are not statistically significant, especially over the Northern Hemisphere. However, model simulations suggest that poleward shift of ocean gyres are most likely to be a consequence of global warming, driven by a systematic poleward displacement of the extratropical atmospheric circulation.

The displacement of extratropical atmospheric circulation has been explored intensively in the past two decades. Investigations have pointed out that two phenomena are related to such a displacement, i.e., positive trends of annular modes (J. Fyfe et al., 1999; Thompson et al., 2000) and expanding tropics (Seidel et al., 2008). Model simulations imply that increasing greenhouse gases (J. Fyfe et al., 1999; Kushner et al., 2001; Cai et al., 2003), ozone depletion over the South Pole (Thompson & Solomon, 2002; Thompson et al., 2011) and increasing aerosols (Allen et al., 2012) over the Northern Hemisphere all contribute to the observed shift in atmospheric circulation, suggesting that human activity is reshaping the climate. However, more recent studies highlighted that the observed climate change is still within the magnitude of natural climate variability (Garfinkel et al., 2015; Allen & Kovilakam, 2017; Waugh et al., 2018; Grise et al., 2019). For example, in the satellite altimetry record, there is an equatorward shift of the Gulf Stream from the 1990s to the 2000s (Fig. 5A), which conflicts with our model simulations. This is because the North Atlantic Oscillation, which regulates the position of the North Atlantic Subtropical Gyre (Joyce et al., 2000; Frankignoul et al., 2001), has shifted to a negative phase during 1990-2010. Nevertheless, from a long-term perspective, our SST based metric and many other studies have demonstrated that the Gulf Stream (or North Atlantic Subtropical Gyre) has experienced an overall northward displacement during the twentieth century (Frankignoul et al., 2001; Yin & Goddard, 2013), which is in line with the model results.

Regarding the rate of the shift, our estimation of the shift of subtropical/subpolar gyres is on the order of $0.1/0.04^\circ$ decade⁻¹ during the past four decades. The estimated rate for tropical expansion is on the order of $0.2\text{--}3.0^\circ$ decade⁻¹, depending on the datasets and methods of analysis (Davis & Rosenlof, 2012). Recent work suggested that the rate of tropical expansion is most likely on the order of 0.2° decade⁻¹, which is consistent with our estimation of the movement of subtropical gyres (Waugh et al., 2018; Paul et al., 2018). Ocean temperature proxy records illustrate that the Agulhas Current was 7° equatorward of its modern position (Bard & Rickaby, 2009) during the glacial period. This implies that the ocean circulation may have shifted significantly since the Last Glacial Maximum (21 ka before present). Considering that the present climate is already relatively warm compared to the last glacial period, the space for ocean gyres to shift in the future may be limited. However, uncertainty also exists in our estimation of the magnitude of the shift due to short term natural climate variability. Since the period of satellite observations is still relatively short, it may take some time before the signal of global warming overcomes natural variability and a robust measurement can be achieved. The proxy record from the Agulhas Current (Bard & Rickaby, 2009) provides a good analogue for detecting the past limit of a circulation shift. We propose that long-term observations combined with more paleoclimate records, in particular over some key regions, such as western boundary currents and the subtropical fronts, will provide a more robust insight on how much the climate zone can shift.

The poleward shift of the major ocean gyres may have broad environmental and societal impacts. There is evidence showing that the western boundary currents are transporting more heat to the mid-latitudes (Yang, Liu, et al., 2016; Yang, Lohmann, et al., 2016). Yin (2005) demonstrated that there is a consistent poleward movement of storm tracks and the jet stream, most likely associated with the change in the subtropical front

induced by ocean gyre movement (Primeau & Cessi, 2001). The eastern boundary of the subtropical gyres, such as the Benguela ecosystem, has also been shrinking over the past three decades (Blamey et al., 2015). The margins of the gyres experience the most significant changes. For example, the Gulf of Maine, located at the north flank of the Gulf Stream, is undergoing vigorous ocean temperature increases even though the Gulf Stream is observed to be weaker (Dima & Lohmann, 2010; Caesar et al., 2018). Such changes have had disastrous consequences for the local cod fishery (Pershing et al., 2015). Similar impacts have also been reported for the Uruguayan and Argentinean industrial fisheries due to enhanced warming at the margins of Southern Atlantic Subtropical Gyre (Auaud & Martos, 2012; Ignacio et al., 2019). The shift in ocean gyres generates a pronounced sea level rise band over the mid-latitudes (Fig. 3) (Yin & Goddard, 2013). This pattern is superimposed on global mean sea level rise, causing an additional threat to the nearby islands and the mainland in the mid-latitudes, for instance, the northeast coast of North America (Yin & Goddard, 2013). The ocean desert is expanding and causing a reduction of total marine productivity (Stramma et al., 2008; Steinacher et al., 2010). Previously, the mechanism was explained by a stronger stratification induced by surface warming (Stramma et al., 2008). Our study reveals that the displacement of the subtropical gyre may be expanding the ocean desert as well. As part of global circulation, the shifting large-scale ocean gyres has the potential to reshape ocean circulation over the tropics, near coastal regions, and also change meridional overturning circulation (Lique & Thomas, 2018). However, to our knowledge, these topics remain poorly studied.

Figure 1. The major ocean gyres and associated climatological conditions. Contour lines represent the barotropic streamfunction. Solid lines indicate clockwise flow, and dashed lines indicate anti-clockwise flow. A. Background shading shows the sea surface height (SSH). Black arrows illustrate the significant features of the currents. B. Background shading represents the horizontal sea surface temperature gradient. Results are based on the last 100 years of the AWI-CM pre-industrial control run. The abbreviations in the figure are list as follows: North Atlantic Subtropical Gyre (NASTG), South Atlantic Subtropical Gyre (SASTG), North Pacific Subtropical Gyre (NPSTG), South Pacific Subtropical Gyre (SPSTG), Indian Ocean Subtropical Gyre (IOSTG), North Pacific Subpolar Gyres (NPSPG), North Atlantic Subpolar Gyres (NASPG) and Antarctic Circumpolar Current (ACC).

Figure 2. Schematic of the method of tracking the meridional variations of ocean gyres. As gyre-related SSH patterns, subtropical fronts and barotropic steamfunction all resemble the shapes of hills. We use the centre of mass of these hills to track the position of ocean gyres. The grey shading box illustrates the region (also shown as grey rectangles in Fig. 3A and 4A) where the integration is performed. These regions are defined primarily based on the climatology position of each parameter, and do not vary over time. Following equation 1, lat is the latitudinal coordinate of each parameter. For the SSH parameter, Δvar represents $SSH - SSH_{min}$ for calculating the position of subtropical gyres, and $SSH - SSH_{max}$ for calculating the position of subpolar gyres. SSH_{min} and SSH_{max} are the regional minimum and maximum SSH within the integrated regions. For the SST parameter, Δvar represents horizontal SST gradient. For the streamfunction parameter, Δvar represents barotropic streamfunction.

Figure 3. Observational (A) and modelled (B) trends (shading) and climatology (contours) of SSH. A: Trends of SSH based on satellite altimetry (1993-2018). The globally averaged sea level rise (8 cm) has been subtracted. Stippling indicates regions where the trends pass the 95% confidence level (Student's t -test). B: Ensemble SSH change in the doubled CO_2 simulations relative to the pre-industrial control simulation carried out by AWI-CM. Stippling indicates areas where the magnitude of the trend is larger than the standard deviation of the variability. The subpanel at the right side of each graph shows the zonally averaged trend (red) and climatology (blue) of SSH, with the subtropical zone highlighted in grey.

Figure 4. Observational (A) and modelled (B) trends (shading) and climatology (contours) of the sea surface temperature gradients. Contours give the SST gradients at level of $0.5^\circ C/100km$. A: Observational trends based on the NOAA Optimum Interpolation Sea Surface Temperature dataset covering 1982-2018. Stippling indicates regions where the trends pass the 95% confidence level (Student's t -test). B: Trend in the doubled CO_2 simulations relative to the pre-industrial control simulation carried out by AWI-CM. Stippling indicates areas where the magnitude of the trend is larger than the standard deviation of the local variability. The subpanel at the right side of each figure shows the zonally averaged trend (red) and climatology (blue) of sea surface temperature gradients, with the subtropical zone highlighted in grey.

Figure 5. Observational (A) and modelled (B) time series of latitudinal variations of the major ocean gyres. A: Grey bars are indices derived from the centre of the regional high and low SSH based on the satellite altimetry record. Coloured lines are estimations derived from the position of subtropical fronts based on the NOAA Optimum Interpolation Sea Surface Temperature dataset. B: Results from the 150 year AWI-CM doubled CO₂ simulations. The estimation is calculated based on the barotropic stream function weighted centre of each gyre. Coloured thin lines represent individual ensemble members. The thick black lines give the ensemble mean variations. The corresponding linear trends (T) are given by the text, in units of degrees per decade. A positive trend indicates a poleward shift. The associated p-values (P) are also given based on the student's *t*-test.

Figure 6. Observational and modelled climatology (contours) and trends (shading) of the zonal component of the near ocean surface wind. A: Ensemble trends of the zonal near ocean surface wind based on the NCEP/NCAR, NCEP/DOE and NERA-Interim reanalysis datasets covering 1979-2018. Stippling indicates regions where the trends pass the 95% confidence level (Student's *t*-test). B: Zonal near ocean surface wind change in the doubled CO₂ simulations relative to the pre-industrial control simulation carried out by AWI-CM. Stippling indicates areas where the magnitude of the trend is larger than the standard deviation of the variability. The subpanel at the right side of each graph shows the zonally averaged climatology (blue) and trend (red) of zonal near ocean surface wind.

Acknowledgments

We thank Gregor Knorr for providing an internal review of this manuscript, and Qiang Wang for clarifying the calculation of dynamic and steric sea level in the AWI-CM. We would also like to acknowledge Nicholas Foukal and another anonymous reviewer for providing constructive comments. This work was supported through grant (Global sea level change since the Mid Holocene: Background trends and climate-ice sheet feedbacks) from the Deutsche Forschungsgemeinschaft (DFG) as part of the Special Priority Program (SPP)-1889 "Regional Sea Level Change and Society" (SeaLevel). Furthermore, thanks to the projects PACMEDY and PalMOD funded through BMBF and the open fund of State Key Laboratory of Loess and Quaternary Geology, Institute of Earth Environment, CAS (SKLLQG1920). The altimeter products were produced by Ssalto/Duacs and distributed by Aviso, with support from Cnes (<http://www.aviso.altimetry.fr/duacs/>). The sea surface temperature data (NOAA_OISST_V2) is provided by the NOAA/OAR/ESRL PSD, Boulder, Colorado, USA, from their website at <https://www.esrl.noaa.gov/psd/>. We acknowledge the World Climate Research Programme's Working Group on Coupled Modelling, which is responsible for CMIP5, and we thank the climate modelling groups (listed in Table S1 of this paper) for producing and making available their model output. For CMIP, the U.S. Department of Energy's Program for Climate Model Diagnosis and Intercomparison provides coordinating support and led development of software infrastructure in partnership with the Global Organization for Earth System Science Portals.

References

- Allen, R. J., & Kovilakam, M. (2017). The Role of Natural Climate Variability in Recent Tropical Expansion. *Journal of Climate*, 30(16), 6329–6350.
- Allen, R. J., Sherwood, S. C., Norris, J. R., & Zender, C. S. (2012). Recent Northern Hemisphere tropical expansion primarily driven by black carbon and tropospheric ozone. *Nature*, 485(7398), 350.
- Archer, C. L., & Caldeira, K. (2008). Historical trends in the jet streams. *Geophysical Research Letters*, 35(8).
- Auad, G., & Martos, P. (2012). Climate variability of the northern Argentinean shelf circulation: impact on *Engraulis anchoita*. *The International Journal of Ocean and Climate Systems*, 3(1), 17–43.
- Bard, E., & Rickaby, R. E. (2009). Migration of the subtropical front as a modulator of glacial climate. *Nature*, 460(7253), 380.
- Blamey, L. K., Shannon, L. J., Bolton, J. J., Crawford, R. J., Dufois, F., Evers-King, H., ... others (2015). Ecosystem change in the southern Benguela and the underlying processes. *Journal of Marine Systems*, 144, 9–29.
- Caesar, L., Rahmstorf, S., Robinson, A., Feulner, G., & Saba, V. (2018). Observed fingerprint of a weakening Atlantic Ocean overturning circulation. *Nature*, 556(7700), 191.
- Cai, W. (2006). Antarctic ozone depletion causes an intensification of the Southern Ocean super-gyre circulation. *Geophysical Research Letters*, 33(3), L03712.
- Cai, W., Whetton, P. H., & Karoly, D. J. (2003). The response of the Antarctic Oscillation to increasing and stabilized atmospheric CO₂. *Journal of Climate*, 16(10), 1525–1538.
- Chen, G., Lu, J., & Frierson, D. M. (2008). Phase speed spectra and the latitude of surface westerlies: Interannual variability and global warming trend. *Journal of Climate*, 21(22), 5942–5959.
- Davis, S. M., & Rosenlof, K. H. (2012). A multidiagnostic intercomparison of tropical-width time series using reanalyses and satellite observations. *Journal of Climate*, 25(4), 1061–1078.
- Dima, M., & Lohmann, G. (2010). Evidence for two distinct modes of large-scale ocean circulation changes over the last century. *Journal of Climate*, 23(1), 5–

16.

- Foukal, N. P., & Lozier, M. S. (2017). Assessing variability in the size and strength of the North Atlantic subpolar gyre. *Journal of Geophysical Research: Oceans*, 122(8), 6295–6308.
- Frankignoul, C., de Coëtlogon, G., Joyce, T. M., & Dong, S. (2001). Gulf Stream variability and ocean–atmosphere interactions. *Journal of physical Oceanography*, 31(12), 3516–3529.
- Fyfe, J., Boer, G., & Flato, G. (1999). The Arctic and Antarctic Oscillations and their projected changes under global warming. *Geophysical Research Letters*, 26(11), 1601–1604.
- Fyfe, J. C., & Saenko, O. A. (2006). Simulated changes in the extratropical Southern Hemisphere winds and currents. *Geophysical Research Letters*, 33(6).
- Garfinkel, C. I., Waugh, D. W., & Polvani, L. M. (2015). Recent Hadley cell expansion: The role of internal atmospheric variability in reconciling modeled and observed trends. *Geophysical Research Letters*, 42(24).
- Goni, G. J., Bringas, F., & DiNezio, P. N. (2011). Observed low frequency variability of the Brazil Current front. *Journal of Geophysical Research: Oceans*, 116(C10).
- Grise, K. M., Davis, S. M., Simpson, I. R., Waugh, D. W., Fu, Q., Allen, R. J., ... others (2019). Recent tropical expansion: natural variability or forced response? *Journal of Climate*, 32(5), 1551–1571.
- Häkkinen, S., & Rhines, P. B. (2004). Decline of subpolar North Atlantic circulation during the 1990s. *Science*, 304(5670), 555–559.
- Hudson, R. (2012). Measurements of the movement of the jet streams at mid-latitudes, in the Northern and Southern Hemispheres, 1979 to 2010. *Atmospheric Chemistry and Physics*, 12(16), 7797–7808.
- Ignacio, G., Leonardo, O., Yamand, M., Alberto, R. P., & Omar, D. (2019). Evidence of ocean warming in Uruguay’s fisheries landings: the mean temperature of the catch approach. *Mar Ecol Prog Ser*. doi: 10.3354/meps13035
- Joyce, T. M., Deser, C., & Spall, M. A. (2000). The relation between decadal variability of subtropical mode water and the North Atlantic Oscillation. *Journal of Climate*, 13(14), 2550–2569.
- Kalnay, E., Kanamitsu, M., Kistler, R., Collins, W., Deaven, D., Gandin, L., ... others (1996). The NCEP/NCAR 40-year reanalysis project. *Bulletin of the American meteorological Society*, 77(3), 437–471.
- Kanamitsu, M., Ebisuzaki, W., Woollen, J., Yang, S.-K., Hnilo, J., Fiorino, M., & Potter, G. (2002). NCEP-DOE AMIP-II Reanalysis (r-2). *Bulletin of the American Meteorological Society*, 83(11), 1631–1643.
- Kushner, P. J., Held, I. M., & Delworth, T. L. (2001). Southern Hemisphere atmospheric circulation response to global warming. *Journal of Climate*, 14(10), 2238–2249.
- Lique, C., & Thomas, M. D. (2018). Latitudinal shift of the Atlantic Meridional Overturning Circulation source regions under a warming climate. *Nature Climate Change*, 8(11), 1013.
- Munk, W. H. (1950). On the wind-driven ocean circulation. *Journal of meteorology*, 7(2), 80–93.
- Nakamura, H., Sampe, T., Tanimoto, Y., & Shimpo, A. (2004). Observed associations among storm tracks, jet streams and midlatitude oceanic fronts. *Earth’s Climate: The Ocean–Atmosphere Interaction, Geophys. Monogr.*, 147, 329–345.
- Norris, J. R., Allen, R. J., Evan, A. T., Zelinka, M. D., ODell, C. W., & Klein, S. A. (2016). Evidence for climate change in the satellite cloud record. *Nature*, 536(7614), 72–75.
- Paul, W. S., Jian, L., Kevin, M. G., Sean, M. D., & Thomas, B. (2018). Re-examining tropical expansion. *Nature Climate Change*, 8, 768–775.

- Pershing, A. J., Alexander, M. A., Hernandez, C. M., Kerr, L. A., Le Bris, A., Mills, K. E., ... others (2015). Slow adaptation in the face of rapid warming leads to collapse of the Gulf of Maine cod fishery. *Science*, 350(6262), 809–812.
- Primeau, F., & Cessi, P. (2001). Coupling between wind-driven currents and midlatitude storm tracks. *Journal of climate*, 14(6), 1243–1261.
- Ridgway, K. (2007). Long-term trend and decadal variability of the southward penetration of the East Australian Current. *Geophysical Research Letters*, 34(13).
- Roemmich, D., Gilson, J., Davis, R., Sutton, P., Wijffels, S., & Riser, S. (2007). Decadal spinup of the South Pacific subtropical gyre. *Journal of Physical Oceanography*, 37(2), 162–173.
- Roemmich, D., Gilson, J., Sutton, P., & Zilberman, N. (2016). Multidecadal change of the South Pacific gyre circulation. *Journal of Physical Oceanography*, 46(6), 1871–1883.
- Saenko, O. A., Fyfe, J. C., & England, M. H. (2005). On the response of the oceanic wind-driven circulation to atmospheric CO₂ increase. *Climate Dynamics*, 25(4), 415–426.
- Scheff, J., & Frierson, D. (2012). Twenty-first-century multimodel subtropical precipitation declines are mostly midlatitude shifts. *Journal of Climate*, 25(12), 4330–4347.
- Seidel, D. J., Fu, Q., Randel, W. J., & Reichler, T. J. (2008). Widening of the tropical belt in a changing climate. *Nature geoscience*, 1(1), 21–24.
- Sen Gupta, A., Santoso, A., Taschetto, A. S., Ummenhofer, C. C., Trevena, J., & England, M. H. (2009). Projected changes to the Southern Hemisphere ocean and sea ice in the IPCC AR4 climate models. *Journal of Climate*, 22(11), 3047–3078.
- Sidorenko, D., Rackow, T., Jung, T., Semmler, T., Barbi, D., Danilov, S., ... others (2015). Towards multi-resolution global climate modeling with ECHAM6–FESOM. Part I: model formulation and mean climate. *Climate Dynamics*, 44(3–4), 757–780.
- Sokolov, S., & Rintoul, S. R. (2009). Circumpolar structure and distribution of the Antarctic Circumpolar Current fronts: 2. Variability and relationship to sea surface height. *Journal of Geophysical Research: Oceans*, 114(C11).
- Steinacher, M., Joos, F., Frölicher, T., Bopp, L., Cadule, P., Cocco, V., ... others (2010). Projected 21st century decrease in marine productivity: a multi-model analysis. *Biogeosciences*, 7(3), 979–1005.
- Stramma, L., Johnson, G. C., Sprintall, J., & Mohrholz, V. (2008). Expanding oxygen-minimum zones in the tropical oceans. *science*, 320(5876), 655–658.
- Taylor, K. E., Stouffer, R. J., & Meehl, G. A. (2012). An overview of CMIP5 and the experiment design. *Bulletin of the American Meteorological Society*, 93(4), 485–498.
- Thompson, D. W., & Solomon, S. (2002). Interpretation of recent Southern Hemisphere climate change. *Science*, 296(5569), 895–899.
- Thompson, D. W., Solomon, S., Kushner, P. J., England, M. H., Grise, K. M., & Karoly, D. J. (2011). Signatures of the Antarctic ozone hole in Southern Hemisphere surface climate change. *Nature Geoscience*, 4(11), 741.
- Thompson, D. W., Wallace, J. M., & Hegerl, G. C. (2000). Annular modes in the extratropical circulation. Part II: Trends. *Journal of climate*, 13(5), 1018–1036.
- Waugh, D. W., Grise, K. M., Seviour, W. J., Davis, S. M., Davis, N., Adam, O., ... others (2018). Revisiting the relationship among metrics of tropical expansion. *Journal of Climate*, 31(18), 7565–7581.
- Wu, L., Cai, W., Zhang, L., Nakamura, H., Timmermann, A., Joyce, T., ... others (2012). Enhanced warming over the global subtropical western boundary currents. *Nature Climate Change*, 2(3), 161–166.
- Yang, H., Liu, J., Lohmann, G., Shi, X., Hu, Y., & Chen, X. (2016). Ocean-

- 438 atmosphere dynamics changes associated with prominent ocean surface tur-
 439 bulent heat fluxes trends during 1958–2013. *Ocean Dynamics*, 66(3), 353–365.
- 440 Yang, H., Lohmann, G., Wei, W., Dima, M., Ionita, M., & Liu, J. (2016). Inten-
 441 sification and poleward shift of subtropical western boundary currents in a
 442 warming climate. *Journal of Geophysical Research: Oceans*, 121(7), 4928–
 443 4945.
- 444 Yin, J. (2005). A consistent poleward shift of the storm tracks in simulations of 21st
 445 century climate. *Geophysical Research Letters*, 32(18).
- 446 Yin, J., & Goddard, P. B. (2013). Oceanic control of sea level rise patterns along
 447 the East Coast of the United States. *Geophysical Research Letters*, 40(20),
 448 5514–5520.

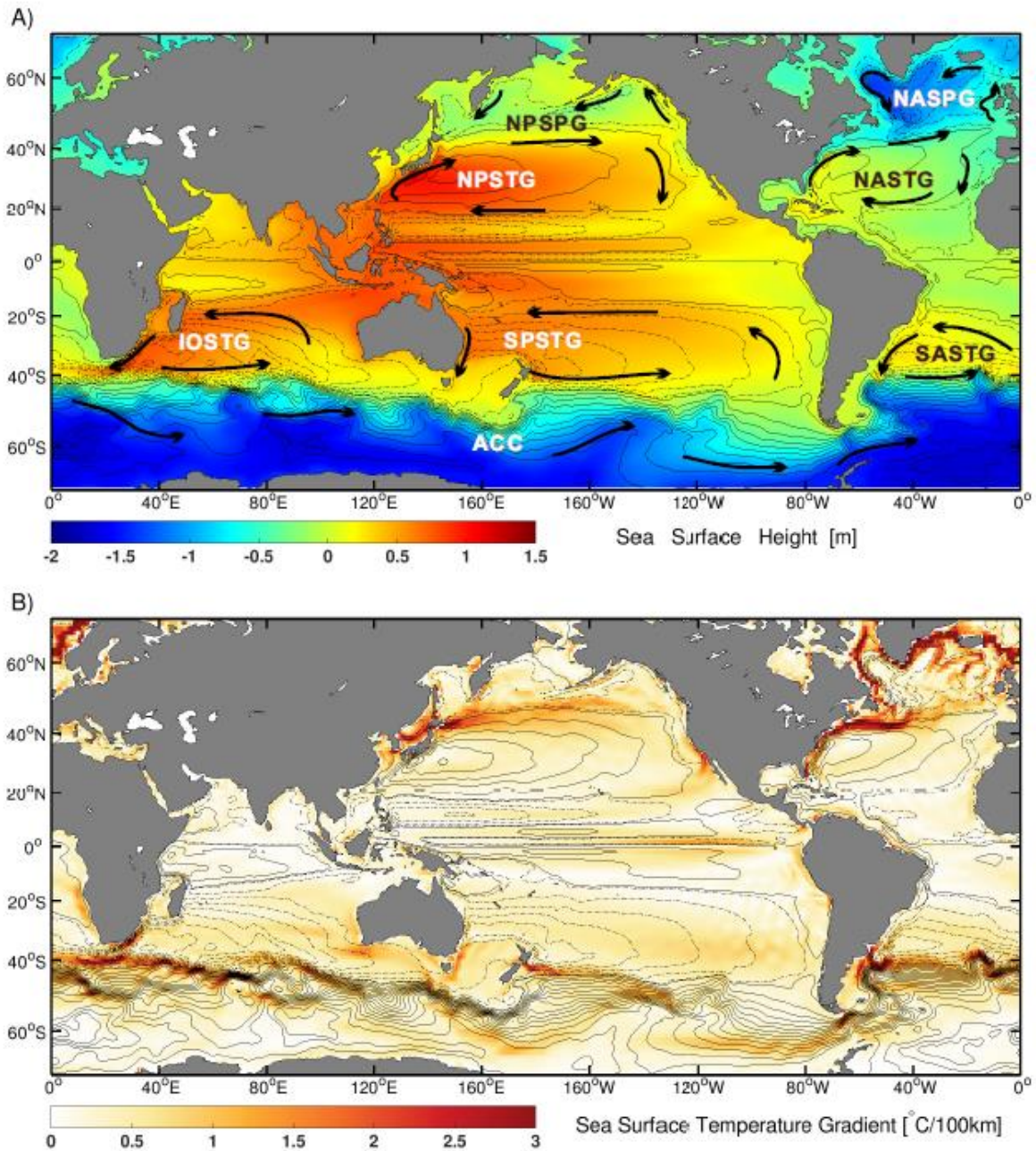


Figure 1. The major ocean gyres and associated climatological conditions. Contour lines represent the barotropic streamfunction. Solid lines indicate clockwise ow, and dashed lines indicate anti-clockwise ow. A. Background shading shows the sea surface height (SSH). Black arrows illustrate the significant features of the currents. B. Background shading represents the horizontal sea surface temperature gradient. Results are based on the last 100 years of the AWI-CM pre-industrial control run. The abbreviations in the figure are list as follows: North Atlantic Subtropical Gyre (NASTG), South Atlantic Subtropical Gyre (SASTG), North Pacific Subtropical Gyre (NPSTG), South Pacific Subtropical Gyre (SPSTG), Indian Ocean Subtropical Gyre (IOSTG), North Pacific Subpolar Gyres (NPSPG), North Atlantic Subpolar Gyres (NASPG) and Antarctic Circumpolar Current (ACC).

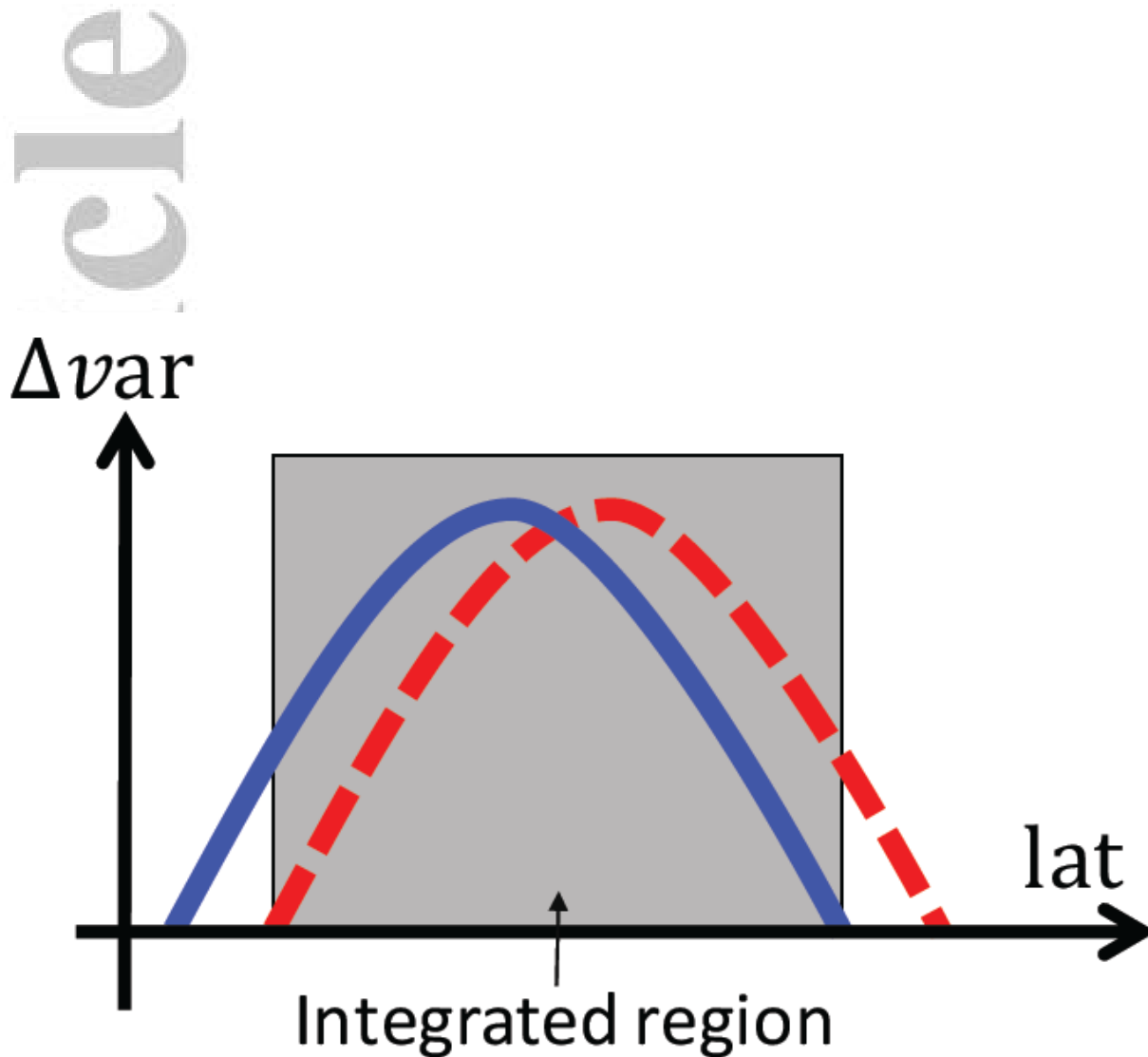


Figure 2. Schematic of the method of tracking the meridional variations of ocean gyres. As gyre-related SSH patterns, subtropical fronts and barotropic streamfunction all resemble the shapes of hills. We use the centre of mass of these hills to track the position of ocean gyres. The grey shading box illustrates the region (also shown as grey rectangles in Fig. 3A and 4A) where the integration is performed. These regions are defined primarily based on the climatology position of each parameter, and do not vary over time. Following equation 1, lat is the latitudinal coordinate of each parameter. For the SSH parameter, Δvar represents $SSH - SSH_{min}$ for calculating the position of subtropical gyres, and $SSH - SSH_{max}$ for calculating the position of subpolar gyres. SSH_{min} and SSH_{max} are the regional minimum and maximum SSH within the integrated regions. For the SST parameter, Δvar represents horizontal SST gradient. For the streamfunction parameter, Δvar represents barotropic streamfunction.

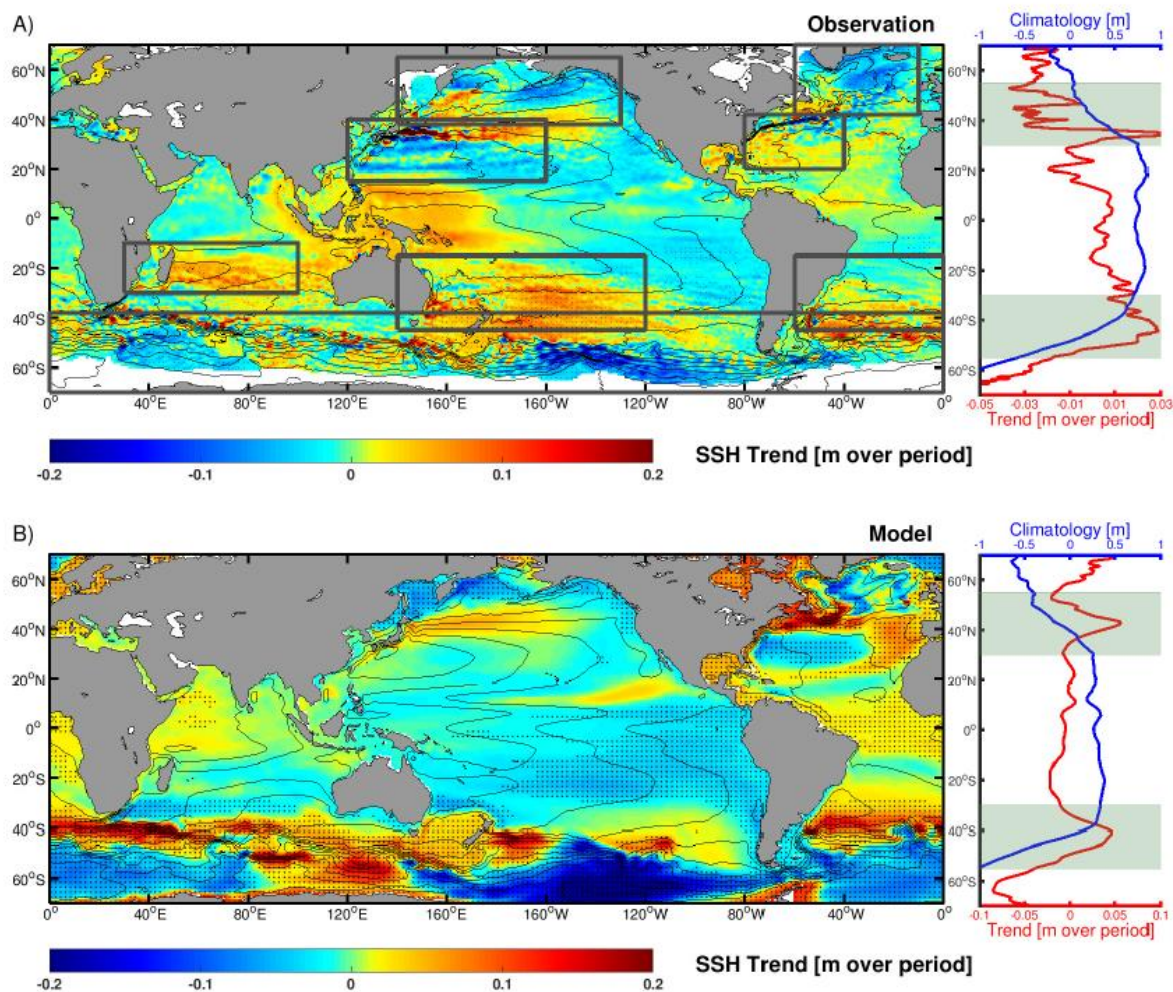


Figure 3. Observational (A) and modelled (B) trends (shading) and climatology (contours) of SSH. A: Trends of SSH based on satellite altimetry (1993-2018). The globally averaged sea level rise (8 cm) has been subtracted. Stippling indicates regions where the trends pass the 95% confidence level (Student's t -test). B: Ensemble SSH change in the doubled CO₂ simulations relative to the pre-industrial control simulation carried out by AWI-CM. Stippling indicates areas where the magnitude of the trend is larger than the standard deviation of the variability. The subpanel at the right side of each graph shows the zonally averaged trend (red) and climatology (blue) of SSH, with the subtropical zone highlighted in grey.

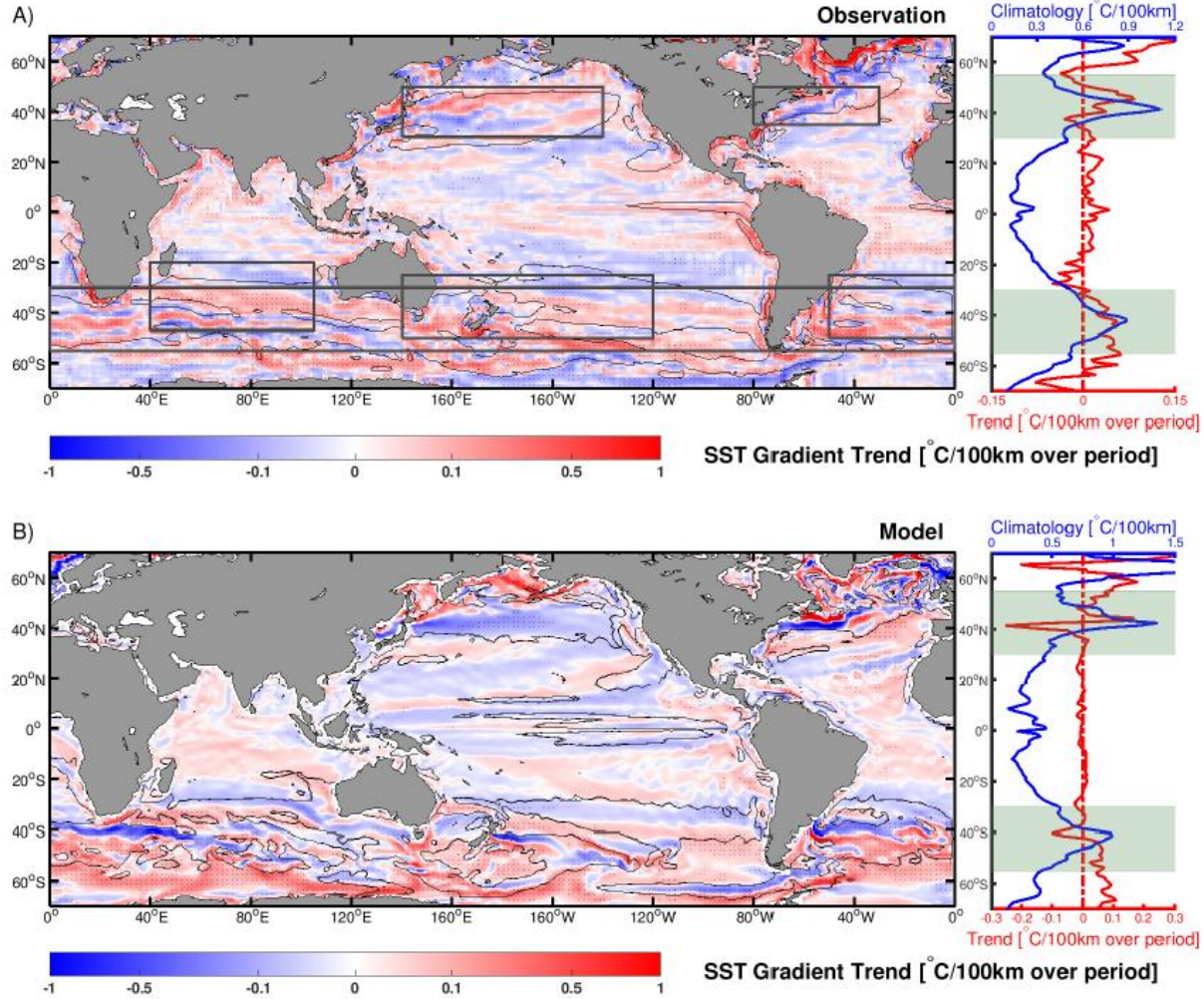
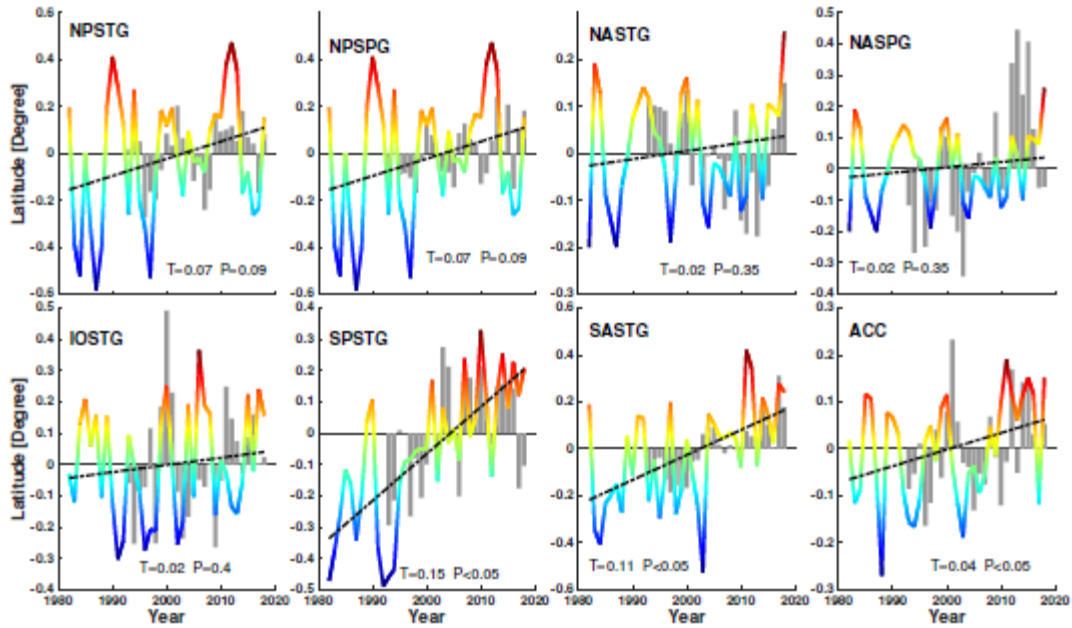


Figure 4. Observational (A) and modelled (B) trends (shading) and climatology (contours) of the sea surface temperature gradients. Contours give the SST gradients at level of $0.5^{\circ}\text{C}/100\text{km}$. A: Observational trends based on the NOAA Optimum Interpolation Sea Surface Temperature dataset covering 1982-2018. Stippling indicates regions where the trends pass the 95% confidence level (Student's t -test). B: Trend in the doubled CO_2 simulations relative to the pre-industrial control simulation carried out by AWI-CM. Stippling indicates areas where the magnitude of the trend is larger than the standard deviation of the local variability. The subpanel at the right side of each figure shows the zonally averaged trend (red) and climatology (blue) of sea surface temperature gradients, with the subtropical zone highlighted in grey.

A) Observation



B) Model

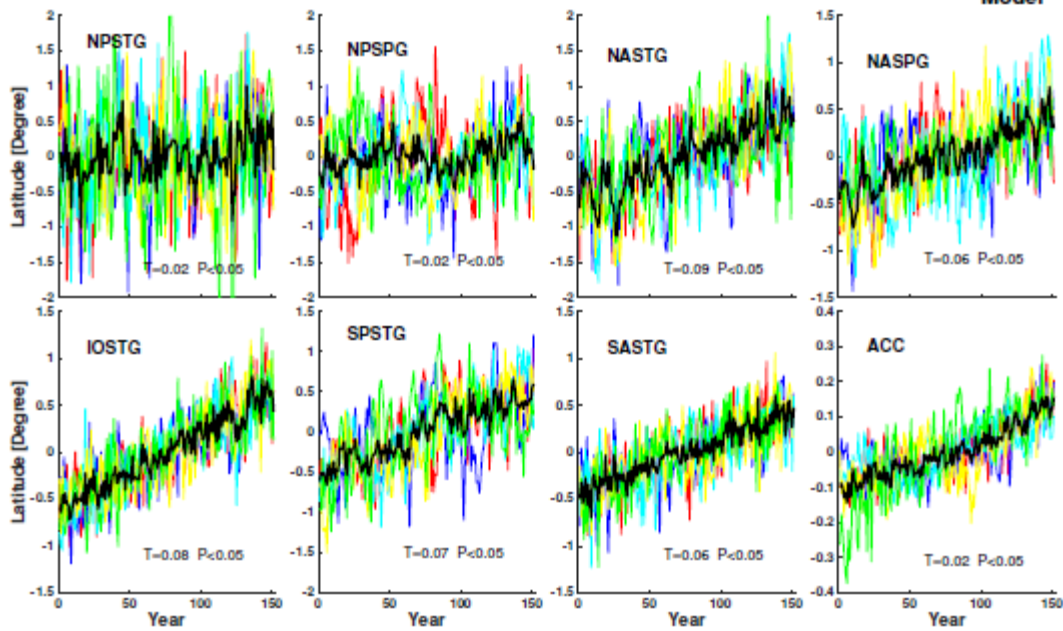


Figure 5. Observational (A) and modelled (B) time series of latitudinal variations of the major ocean gyres. A: Grey bars are indices derived from the centre of the regional high and low SSH based on the satellite altimetry record. Coloured lines are estimations derived from the position of subtropical fronts based on the NOAA Optimum Interpolation Sea Surface Temperature dataset. B: Results from the 150 year AWI-CM doubled CO₂ simulations. The estimation is calculated based on the barotropic stream function weighted centre of each gyre. Coloured thin lines represent individual ensemble members. The thick black lines give the ensemble mean variations. The corresponding linear trends (T) are given by the text, in units of degrees per decade. A positive trend indicates a poleward shift. The associated p-values (P) are also given based on the student's *t*-test.

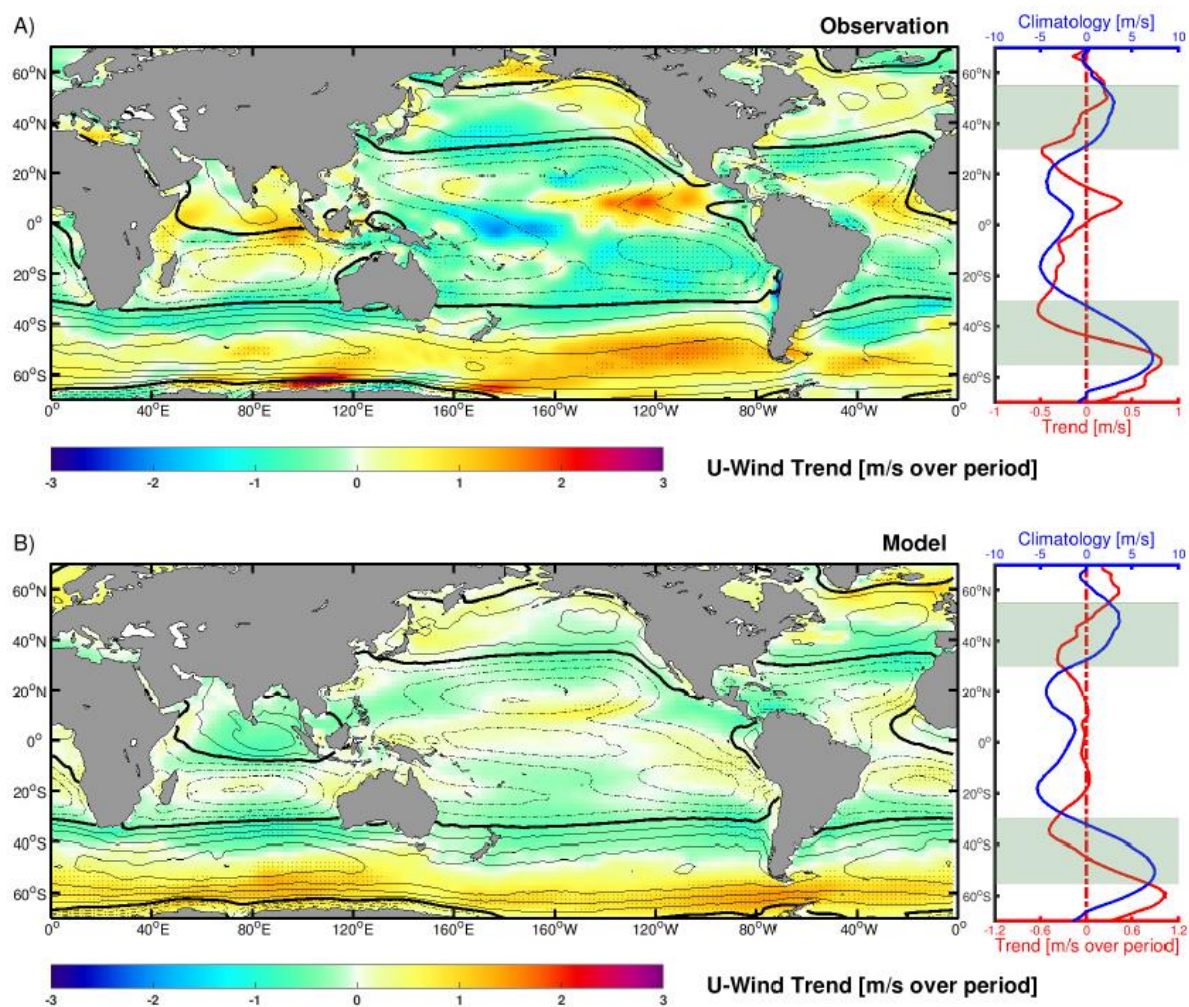


Figure 6. Observational and modelled climatology (contours) and trends (shading) of the zonal component of the near ocean surface wind. A: Ensemble trends of the zonal near ocean surface wind based on the NCEP/NCAR, NCEP/DOE and NERA-Interim reanalysis datasets covering 1979-2018. Stippling indicates regions where the trends pass the 95% confidence level (Student's *t*-test). B: Zonal near ocean surface wind change in the doubled CO₂ simulations relative to the pre-industrial control simulation carried out by AWI-CM. Stippling indicates areas where the magnitude of the trend is larger than the standard deviation of the variability. The subpanel at the right side of each graph shows the zonally averaged climatology (blue) and trend (red) of zonal near ocean surface wind.